HHS Public Access

Author manuscript

Pediatr Res. Author manuscript; available in PMC 2014 September 27.

Published in final edited form as:

Pediatr Res. 2013 November ; 74(5): 494–502. doi:10.1038/pr.2013.147.

Heterotaxy-spectrum heart defects in *Zic3* hypomorphic mice

Allison M. Haaning[1], **Malgorzata E. Quinn**[1], and **Stephanie M. Ware**[1]

[1]Cincinnati Children's Hospital Medical Center, Division of Molecular Cardiovascular Biology, Cincinnati, OH

Abstract

Background—Mutations in ZIC3 cause X-linked heterotaxy and isolated cardiovascular malformations. Recent data suggest a potential cell-autonomous role for Zic3 in myocardium via regulation of *Nppa* and *Tbx5*. We sought to develop a hypomorphic *Zic3* mouse to model human heterotaxy and investigate developmental mechanisms underlying variability in cardiac phenotypes.

Methods—*Zic3* hypomorphic mice were created by targeted insertion of a neomycin cassette and investigated by gross, histologic, and molecular methods

Results—Low level *Zic3* expression is sufficient for partial rescue of viability as compared to *Zic3* null mice. Concordance of early left-right molecular marker abnormalities and later anatomic abnormalities suggests the primary effect of Zic3 in heart development occurs during left-right patterning. Cardiac specific gene expression of *Nppa* (ANF) and *Tbx5* marked the proper morphological locations in the heart regardless of looping abnormalities.

Conclusions—*Zic3* hypomorphic mice are a useful model to investigate the variable cardiac defects resulting from a single genetic defect. Low level *Zic3* expression rescues the left pulmonary isomerism identified in *Zic3* null embryos. Our data do not support a direct role for Zic3 in the myocardium via regulation of *Nppa* and *Tbx5* and suggest the primary effect of Zic3 on cardiac development occurs during left-right patterning.

INTRODUCTION

Patterning of the left-right axis is an event in early vertebrate development that is necessary for proper organ asymmetry. Signaling pathways involved in left-right patterning are conserved in vertebrates, and perturbation of genes encoding proteins in these pathways lead to abnormal organ patterning and arrangement known as situs ambiguus or heterotaxy. Mutations in *Zinc Finger Protein of the Cerebellum 3* (*ZIC3*) were the first genetic cause of heterotaxy identified in humans [1,2], accounting for about one percent of sporadic and 75 percent of X-linked familial heterotaxy cases [3]. ZIC3 is a member of the ZIC family of

CORRESPONDING AUTHOR: Stephanie M. Ware, MD, PhD, Cincinnati Children's Hospital Medical Center, Division of Molecular Cardiovascular Biology, 240 Albert Sabin Way, Cincinnati, OH 45229-3039, Phone: 513-636-9427, Fax: 513-636-5958, stephanie.ware@cchmc.org.

DISCLOSURE: There are no disclosures or conflict of interest.

transcription factors, which are related to GLI proteins that mediate hedgehog signaling, a conserved developmental pathway important for left-right patterning [4]. ZIC3 is able to bind and activate transcription at the GLI binding site [5–8], and we recently demonstrated that ZIC3 converts GLI3 from repressor to activator in vitro [9]. In addition, we identified that Zic3 regulates limb digit number via its modifying effect on Gli3 and Shh expression levels. It has been surmised that ZIC3 may similarly affect left-right signaling through its possible involvement in Shh signaling [10,11]. Zic3 has also been shown to affect a conserved TGFβ signaling pathway important for left-right signaling via interaction with the ligand nodal. A genetic interaction is demonstrated by a more severe phenotype in *Zic3*/*Nodal* compound mutants. In addition, reduced expression of a *Nodal* enhancer-driven β-galactosidase transgene at the node in *Zic3* null mice [12], and abnormal *Nodal* expression in *Zic3* null mice [11] indicate disruption of this critical pathway by loss of function of Zic3. Proper left-right patterning also requires an intact midline, and *Zic3* null mice exhibit a range of midline defects such as disrupted notochord formation, incomplete neural tube closure, vertebral malformations, and bent tails [11,13]. The exact mechanism by which Zic3 patterns the left-right axis remains unknown, but its role in left-right patterning is clearly essential and is conserved in human, mouse, zebrafish, and frog [1,3,10,11,13–15].

Isolated cardiovascular malformations have been observed in patients with ZIC3 mutations[3,16–19], indicating that there may be a requirement for ZIC3 specifically in the heart, and separate from its role in left-right patterning, for proper cardiovascular development. Recently, ZIC3 was shown to bind to serum response factor (SRF) and synergistically co-activate important cardiac genes including *Nppa* (encoding ANF), *Tbx5*, and *Nkx2.5 in vitro* [20]. In that study, *Zic3* was shown to be expressed in the developing mouse heart by RT-PCR; however, the question of whether *Zic3* is expressed at physiological levels in the developing heart has not been resolved since other studies show no detectable *Zic3* gene expression during cardiogenesis by whole mount in situ hybridization (WISH)[5,11]. Thus a potential role for Zic3 in the cardiac compartment remains controversial. A wide phenotypic variety of laterality-spectrum heart defects, such as transposition of the great arteries (TGA), atrial isomerism, and atrioventricular (AV) septal defects have been observed in *Zic3* null mice [11–14,20]; however, because of early embryonic lethality secondary to gastrulation defects [21], it is difficult to collect adequate numbers of embryos with abnormal heart development to study laterality-spectrum heart defects. Here we present *Zic3* hypomorphic mice that have low early embryonic lethality and high penetrance of laterality-spectrum heart defects as a model to better understand the etiology of cardiovascular malformations.

RESULTS

Analysis of *Zic3* expression

Targeted insertion of a neomycin cassette into intron 1 of murine *Zic3* (Figure 1A), which is located on the X chromosome, results in a hypomorphic allele, $Zic3^{NeoIn1}$. Embryos containing only the $Zic3^{NeoIn1}$ allele ($Zic3^{NeoIn1/NeoIn1}$ or $Zic3^{NeoIn1/y}$ genotypes), which will hereafter be referred to as *Zic3* hypomorphs, were shown to have a universal reduction of *Zic3* expression by real-time RT-PCR (qPCR) (Figure 1B). The mean *Zic3* expression

level in embryonic day (E) 12.5 *Zic3* hypomorphs was 4.7% compared to wild-type embryos (n=3 for each genotype) by qPCR. These low levels of *Zic3* expression were not able to be detected by whole mount *in situ* hybridization (WISH) at E9.5 and E10.5 (Figure 2A, B and data not shown).

Zic3 expression has been detected in E10.5 hearts by qPCR and RT-PCR in previous studies [5,20] and recent work suggests a possible novel role in the ventricular myocardium via regulation of ANF expression [20]; however, its expression has not been detected in the heart at any embryonic stage by WISH [12]. Previously, we described the generation of *Zic3*-LacZ-BAC reporter transgenic mice for more sensitive detection of Zic3 expression during development [9] and we therefore sought to determine whether reporter gene expression was detectable in the cardiac compartment *in vivo*. Eight *Zic3*-LacZ-BAC transgenic lines were analyzed, and all lines had similar expression patterns from E6.5–E12.5, which were also comparable to *Zic3* WISH expression patterns from E6.5–E12.5. At least three lines were analyzed at each of the following stages: E6.5, E8, E8.5, E9.5, E10.5, E11.5, and E12.5; Embryos were embedded and sectioned in order to analyze cardiac expression. *Zic3* expression was not detected in the heart in any *Zic3*-LacZ-BAC line during embryonic development. A representative E12.5 *Zic3*-LacZ-BAC embryo is shown (Figure 2C), exhibiting no expression of β-galactosidase in the whole (Figure 2D) or sectioned (Figure 2E) heart.

Phenotypic analysis of Zic3 Hypomorphs

Reduced expression of *Zic3* led to phenotypes in embryonic and adult mice that were similar to those seen in *Zic3* null mice[11,21]. Like *Zic3* null mice, *Zic3* hypomorphs exhibited gastrulation defects, delayed growth, craniofacial defects, neural tube closure defects, and a variety of laterality defects (Figure 3). *Zic3* hypomorphs exhibited very modest embryonic or fetal lethality (Table 1), making them a useful model for studying complex cardiovascular malformations during and after cardiac looping. In addition, the *Zic3* hypomorphs show a decreased rate of phenotypic abnormalities at early stages as compared to *Zic3* nulls. Fifty-one percent of hypomorph females show phenotypic abnormalities prior to E9.5 (Table 1) as compared to 81% of null females at the same stage [21]. Males show a similar difference between hypomorphs (41% phenotypically abnormal) and nulls (61% abnormal[21]).

The most common defects observed in gastrulating *Zic3* hypomorphs were constriction between embryonic and extraembryonic tissue and accumulation of tissue in the proamniotic cavity (Figure 3B, arrow), which are the same defects seen in *Zic3* nulls. In *Zic3* nulls, the tissue in the amniotic cavity (Figure 3B, arrowhead) was previously shown to be mesoderm by WISH, using the mesodermal markers *T-brachyury*, *Fgf8*, and *Wnt3a* [21]. This tissue was also shown to be mesoderm in *Zic3* hypomorphs by *Fgf8* WISH (data not shown). Accumulation of mesoderm tissue in the proamniotic cavity shows that mesoderm tissue is properly specified but that it is unable to incorporate into a definitive germ layer, which is required for completion of gastrulation and proper embryonic patterning [22,23]. Despite the appearance of gastrulation defects, most *Zic3* hypomorphs are able to survive past gastrulation (Table 1).

Growth retardation or delay of most hypomorphs was apparent at earlier embryonic stages by smaller body size and reduced somite number compared to wild-type siblings (Figure 3D); however, a size difference was typically not discernable at later embryonic stages (E14.5–17.5). Neural tube closure defects were observed in 25% of hypomorphs from E12.5–E17.5 (n=58). The main types of neural tube closure defects observed were anterior neural tube defects including exencephaly. The appearance of neural tube closure defects did not correlate with the appearance of laterality defects.

Because of increased survival of *Zic3* hypomorphs as compared to *Zic3* nulls [21], a detailed analysis of laterality and cardiac defects was performed. Laterality defects were observed at early embryonic stages by left-sided marker analysis (Figure 4) or heart looping abnormalities (Figure 5, Table 2) and at later embryonic or fetal stages by complex heart defects (Figure 6, Table 3) and abnormal patterning or positioning of organs as discussed in detail in the following sections. Normal arrangement (situs solitus), abnormal arrangement (situs ambiguus), and right isomerism of organs were observed in hypomorphs at E17.5. Six litters were analyzed at E17.5, containing a total of 18 *Zic3* hypomorphs. Of these, 8 exhibited normal laterality (situs solitus), 3 exhibited right isomerism, and 7 exhibited situs ambiguus. Right isomerism was identified by bilateral, multi-lobed lungs (Figure 3J) and a small or absent spleen. Stomach positioning was random in embryos with right isomerism (Table 3). Situs ambiguus was identified by abnormal lung lobation and/or malpositioning of at least one visceral organ.

Left-right marker analysis in *Zic3* Hypomorphs

Nodal and *Pitx2* markers were analyzed by WISH to identify abnormalities in conserved left-right signaling pathways. *Nodal* is expressed at head fold stages symmetrically in perinodal crown cells. Later, *Nodal* expression is asymmetrical, with increased expression on the left side of the node. At four- to six-somite stages, *Nodal* is also expressed in the left lateral plate mesoderm (LPM). *Pitx2* is first expressed in the left LPM around the same time as *Nodal*, but its expression persists much later. Embryos were collected from E7.75 to E9.5 to attain comparable numbers and stages of WTs and *Zic3* hypomorphs for left-right marker analysis by *Nodal* and *Pitx2* WISH. Embryos that were early head fold (EHF) to six-somite stages were used for *Nodal* WISH, and embryos that were six- to twelve-somite stages were used for *Pitx2* WISH.

Perinodal *Nodal* staining was present in 6/7 and absent in 1/7 (14%) *Zic3* hypomorphs at EHF stage, with robust staining in the 6 embryos with staining present. Perinodal *Nodal* staining was present in 11/17 and absent in 6/17 (35%) one- to three-somite stage embryos, with clearly attenuated staining in 10/11 embryos with staining present. On the contrary, robust *Nodal* staining was present around the nodes of all 16 WT embryos at EHF to three-somite stages. At four- to six-somite stages, only one *Zic3* hypomorph exhibited bilateral *Nodal* expression around the node, and the remaining 17 embryos exhibited no *Nodal* expression around the node (Figure 4B, 4G). Of the 13 WT embryos analyzed at these stages, 10 exhibited greater expression of *Nodal* on the left side of the node; two exhibited symmetrical, bilateral expression; and only one exhibited no expression (Figure 4G). These results were similar to those previously described in *Zic3* nulls and heterozygotes, in which

Nodal expression was normally initiated around the node but often failed to persist past the two-somite stage [11]. These results indicate that there is a threshold requirement for *Zic3* expression to maintain *Nodal* expression at the node. At these same stages, *Nodal* was expressed in the left LPM of 11 of 13 WT embryos analyzed and absent in the remaining two embryos (Figure 4H). However, *Nodal* expression was absent in the LPM of 11 of 18 *Zic3* hypomorphs and present in the left LPM of only 7 hypomorphs (Figure 4H). In contrast to previous results in *Zic3* null embryos in which *Nodal* expression was found in bilateral LPM or right LPM, these patterns of misexpression were never identified in *Zic3* hypomorphs at the same stage (n=18). *Pitx2* was expressed in the left LPM of all 29 WT embryos and in 24 of 45 *Zic3* hypomorphic embryos analyzed. Of the remaining hypomorphs, 47% had abnormal *Pitx2* expression patterns: 14 had bilateral LPM expression, 3 had right-sided LPM expression, and 4 had absent LPM expression (Figure 4I).

Cardiovascular malformations in *Zic3* Hypomorphs

Human heterotaxy demonstrates widely variable cardiac phenotypic presentations, and it was therefore of interest to determine the spectrum of defects identified in these mice with a uniform genetic etiology. Cardiovascular malformations were observed from E8.5 to E17.5. At E9 to E9.5 the most common malformations observed grossly were looping defects, such as leftward (L-) looping or incomplete rightward (D-) looping, or failure of the heart tube to begin differentiating into chambers (Table 2). By E10.5 to E11.5, the malformations observed were more complex, and many hearts contained multiple malformations, the most common being inferior/superior ventricular arrangement, the appearance of a single ventricle, and L-looping (Table 2). Pericardial edema was also observed in several embryos at these stages, indicating cardiac failure. Malformations observed at E12.5–14.5 were similar to those at E10.5–11.5, but by this stage the formation of a single atrium was also observed in some embryos (Table 2).

Zic3 has been previously implicated in having a direct role in cardiac development separate from its role in left-right development[20]. It was reported that *Zic3* null mice have severely reduced expression of ANF (encoded by *Nppa*) and reduced trabecular myocardium. Furthermore, it was reported that *Zic3* null embryonic stem (ES) cells have reduced expression of cardiac-specific genes *Nppa*, *Nkx2.5*, and *Tbx5*, compared to wild-type ES cells[20]. In contrast, analysis of *Nppa* and *Tbx5* gene expression by WISH at E9.5 in our study revealed expression levels in *Zic3* null or hypomorphic embryos (n=4 for each gene) that were qualitatively comparable to wild-type embryos (Figure 5). Furthermore, analysis of hearts at E17.5 in *Zic3* hypomorphs revealed normal trabecular myocardium compared to wild-type (Figure 6).

In addition to being expressed at relatively normal levels, *Nppa* and *Tbx5* also marked the proper morphological locations in the heart regardless of looping abnormalities. *Tbx5* is normally expressed in the left ventricle, and it was expressed in the morphological left ventricle of an L-looped heart (Figure 5B) and along the posterior edge of the ventricle in hearts with single ventricles (Figure 5C), which is the same expression pattern seen with other left ventricular markers, such as *Nppa* and *Hand1*, in single ventricle-containing hearts[12,24,25]. *Nppa* is expressed in the outflow tract, left ventricle, and atria at E9.5; and it

was expressed in the proper morphological locations in *Zic3* nulls (Figure 5E, F). The hearts of *Zic3* hypomorphs were also analyzed by *Nppa* WISH, and expression was seen in the proper morphological locations with levels comparable to wild-types. *Nppa* localization was useful for identifying the region specified as left ventricle in tubular hearts without chamber formation at E9.5 (Figure 5H) and for identifying specific chambers in hearts with very complex looping abnormalities at E11.5 (Figure 5K).

At E17.5 18/46 embryos were *Zic3* hypomorphs (39%), of which 10 had morphological heart defects (56%) (Table 3). The remaining 8 hypomorphs had normal organ asymmetry, heart morphology, and proper levocardial positioning in the chest comparable to wild-type controls (Figure 6A–F). Two hypomorphs with pulmonary and abdominal reversal had hearts with dextrocardial positioning in the chest and anteriorly-positioned aortas (Figure 6G–I). Sectioning of hearts revealed double-outlet right ventricle (DORV) with subaortic ventricular septal defects (VSD) (Figure 6J–L). The three hypomorphs with right isomerism sequence had hearts with mesocardial positioning in the chest, right atrial isomerism and transposition of the great arteries (TGA) (Figure 6M–O). Sectioning of hearts revealed bilateral symmetrical venous valves and atrioventricular septal defects (AVSD) (Figure 6P–R). The four remaining hypomorphs had variable heart phenotypes, as described in Table 3.

DISCUSSION

Heterotaxy is the most highly heritable heart defect [26]. Although the genetic causes are not identified in the majority of patients with heterotaxy, mutations in the zinc finger transcription factor ZIC3 are the known cause of the X-linked form of heterotaxy. The spectrum of cardiovascular malformations identified in patients with heterotaxy, including those with ZIC3 mutations, is broad and an understanding of the mechanistic basis for this range of developmental defects is lacking. In this paper we identify a new hypomorphic *Zic3* mouse created by targeted insertion of a neomycin cassette and demonstrate the utility of this model for investigating molecular and pathologic effects of decreased *Zic3* expression. In contrast to recently published work, our data do not support a novel role for Zic3 in the myocardium via regulation of *Nppa* and *Tbx5* and suggest that the primary effect of Zic3 on cardiac development occurs during left-right patterning stages.

It is not uncommon for insertion of loxP sites and selectable markers to result in hypomorphic alleles which are instructive about gene function [27–29]. Previously, *Nodal* hypomorphs illustrated the role of Nodal in left-right patterning because they circumvented the gastrulation stage lethality identified in *Nodal* null mice. Similarly, *Zic3* hypomorphs prove to be a more useful model for studying cardiac defects than *Zic3* nulls because there is less early lethality resulting from gastrulation defects. Unlike *Nodal* null mice, which never survive past gastrulation, a subset of *Zic3* null mice are able to survive past gastrulation and be born as healthy, fertile adults. There was a higher penetrance of grossly detectable heart defects in *Zic3* hypomorphs (38%, n=24) at E12.5 compared to those previously described in *Zic3* nulls [14]. Furthermore, at E17.5, the penetrance of cardiovascular defects was even higher in *Zic3* hypomorphs (56%, n=18, six litters) than that seen grossly at E12.5 and was associated with increasing complexity of the heart and remodeling of the great arteries. The higher penetrance in hypomorphs at later versus earlier stages may, in part, result from more

sensitive detection based on full histological analysis in all fetuses. On the contrary, very few *Zic3* null embryos survive to these later stages, and few survivors have morphologically abnormal hearts [14]. Thus the *Zic3* hypomorphic mice represent a useful model to better understand the developmental basis of the variable cardiac phenotypes identified in heterotaxy disorders.

Analyses of molecular markers of left-right patterning in *Zic3* hypomorphs demonstrate some important differences as compared to *Zic3* null embryos. In *Zic3* hypomorphs, a higher percent of embryos have normal left-sided *Nodal* expression in the left LPM than in *Zic3* nulls (40% vs. 20%). In addition, *Nodal* is never identified in the right LPM or bilaterally in *Zic3* hypomorphs despite analysis of nearly four-fold more embryos than *Zic3* nulls at the same stages. This partial rescue of left-right signaling by low levels of *Zic3* expression in the hypomorphs suggests a threshold or dose-related response of *Nodal* in the LPM to *Zic3*.

When comparing early left-right patterning molecular marker abnormalities with later anatomic abnormalities, we note that there is strong concordance between abnormal *Pitx2* expression at six- to twelve-somites (53%, n=45) and abnormal anatomy at E17.5 (56%, n=32). These results suggest that if Zic3 has a later role in cardiac development separate from its role in left-right patterning, it accounts for a minority of the identified abnormalities.

Anatomic differences were noted between *Zic3* hypomorphs and *Zic3* null mice at fetal stages analogous to the results seen with earlier stage molecular markers. Left pulmonary isomerism was not observed in any hypomorph, whereas *Zic3* nulls exhibit both right and left pulmonary isomerism and pulmonary reversal[11]. Because the lungs are the only organs to appear asymmetric at the earliest stages of their development[30], it is possible that bilateral misexpression of *Nodal*, and not *Pitx2*, in the LPM causes left pulmonary isomerism. Indeed, in different mouse models exhibiting left pulmonary isomerism, *Nodal* is misexpressed bilaterally in the LPM [31–33].

To further address a possible role for Zic3 in the cardiac compartment, cardiac expression was analyzed by WISH or in multiple *Zic3*-LacZ-BAC transgenic mouse lines, but no detectable gene expression was identified. These data, combined with the normal expression of cardiac markers *Tbx5* and *Nppa*, normal myocardial trabeculation at later stages, and concordance of the penetrance of left-right marker molecular abnormalities and later stage organ abnormalities suggests that heart defects in *Zic3* null and hypomorphic mice are secondary to left-right patterning defects. This has been further supported by two recent studies utilizing conditional approaches to eliminate Zic3 expression in the cardiac compartment [34,35]. *Zic3* hypomorphic mice are a useful model for analyzing laterality-spectrum heart defects, and they will be used in future studies to further investigate the etiology of heart defects associated with Zic3 loss of function.

METHODS

Gene Targeting

An approximately 12 kb region was sub-cloned from a 129 BAC clone that included the *Zic3* locus, and a pGKNeo cassette was incorporated so that a single loxP site was inserted upstream of *Zic3* exon 1 and a loxP/FRT-flanked Neo cassette was inserted downstream of exon 1 in the first intron (Figure 1A). The targeting vector was confirmed by sequencing and then electroporated into C57BL6/129 ES cells for gene targeting by homologous recombination. Properly targeted ES cells were injected into C57BL6 blastocysts, and resulting chimeras were bred with C57BL6 mice to achieve germline transmission, which was verified by southern blot analysis (data not shown). Floxed mice carrying the Neo cassette within intron 1 are referred to as $Zic3^{NeoIn1/WT}$.

Embryo collection and genotyping

All animal experiments conformed with the Guide for the Care and Use of Laboratory Animals published by the U.S. National Institutes of Health and were approved by the Institutional Animal Care and Use Committee of Cincinnati Children's Hospital Medical Center.

Mice were euthanized by CO_2 inhalation, followed by cervical dislocation. E7.5 to 17.5 mouse embryos were collected following timed matings of $Zic3^{NeoIn1/WT}$ females with $Zic3^{NeoIn1/y}$ males ($Zic3^{NeoIn1/NeoIn1}$ females are infertile). Because *Zic3* hypomorphs are often delayed compared to wild-type siblings, pre-somitic stages were matched by Theiler criteria and post-somitic stages were matched by somite number. Embryos were genotyped using primers to detect SRY [11] and the following primers that differentiate between wild-type and hypomorphic *Zic3* alleles: SDL1: 5′-CGT TCT CAA GGT GGT GAG GCA GCA G-3′ and SDL2: 5′-GAA AGG GAT CCG CCG GGT TTG CG-3′.

Embryo processing

Embryos were fixed in four percent paraformaldehyde/PBS (Electron Microscopy Sciences, Hatfield, PA) prior to whole-mount *in situ* hybridization (WISH) and β-galactosidase detection, which was performed as previously described[14].

The organ arrangement and external heart phenotype was observed in E17.5 hypomorphs before the heart was removed for embedding. Prior to embedding, hearts were fixed in four percent paraformaldehyde/PBS and dehydrated into ethanol. Hearts were then washed with xylene for 15 min, 1:1 xylene/paraffin wax for 20 min, and then three times in paraffin wax for one hour per wash. Hearts were embedded in paraffin wax with the apex of the heart oriented toward the top of the block. Hearts were cut transversely into 12 μM sections from apex to aortic arch (posterior to anterior). Sections were stained with hematoxylin and eosin.

Analysis of gene expression

WISH was performed as described previously[11]. For real-time RT-PCR, whole E12.5 embryos were collected in RNA*later* (Ambion, Austin, TX). RNA extractions were performed using a Totally RNA kit (Ambion). cDNA was generated using a High-Capacity

cDNA Reverse Transcription Kit (Applied Biosystems, Foster City, CA). Real-time PCR was performed using an ABI PRISM 7000 Sequence Detection System (Applied Biosystems) and *Power* SYBR Green PCR Master Mix (Applied Biosystems), with intron spanning primer pairs. *Zic3* gene expression results were normalized to *GAPDH*. The following primers were used: GAPDH-F 5′-TGCGACTTCAACAGCAACTC and GAPDH-R 5′-GCCTCTCTTGCTCAGTGTCC; Zic3-F1 5′ – CGGGCTGCGGGAAGAT and Zic3-R1 5′ – CTCACCTGTATGGGTCCTCTTGT; Zic3-F2 5′ – CCCTGCGCAAACACATGA and Zic3-R2 5′ – GGGAGGAATCTGACCCTTGAG.

Two sets of primer pairs for *Zic3*, flanking intron 1 (Zic3 F1/Zic3 R1) and intron 2 (Zic3 F2/Zic3 R2), were used independently for double verification of the *Zic3* expression results. Six independent reactions were run for each biological sample with each of the three primer pairs. Histograms represent relative expression ± standard error.

Acknowledgments

STATEMENT OF FINANCIAL SUPPORT: This work was supported by the National Institutes of Health (grants R01 HL088639 and R01 HL088639-03S1 to SMW).

We thank B. Bruneau for *Nppa* and *Tbx5 in situ* probes. We thank R.B. Hinton for helpful discussions on cardiac malformations in heterotaxy.

References

1. Gebbia M, Ferrero GB, Pilia G, et al. X-linked *situs* abnormalities result from mutations in Zic 3. Nature Genet. 1997; 17:305–8. [PubMed: 9354794]
2. Sutherland MJ, Ware SM. Disorders of left-right asymmetry: heterotaxy and situs inversus. Am J Med Genet C Semin Med Genet. 2009; 151C:307–17. [PubMed: 19876930]
3. Ware SM, Peng J, Zhu L, et al. Identification and functional analysis of ZIC3 mutations in heterotaxy and related congenital heart defects. Am J Hum Genet. 2004; 74:93–105. [PubMed: 14681828]
4. Aruga J, Nagai T, Tokuyama T, et al. The mouse Zic gene family. J Biol Chem. 1996; 271:1043–7. [PubMed: 8557628]
5. Bedard JE, Haaning AM, Ware SM. Identification of a Novel ZIC3 Isoform and Mutation Screening in Patients with Heterotaxy and Congenital Heart Disease. PLoS One. 2011; 6:e23755. [PubMed: 21858219]
6. Mizugishi K, Aruga J, Nakata K, Mikoshiba K. Molecular properties of Zic proteins as transcriptional regulators and their relationship to GLI proteins. J Biol Chem. 2001; 276:2180–8. [PubMed: 11053430]
7. Aruga J, Yokota N, Hashimoto M, Furuichi T, Fukuda M, Mikoshiba K. A novel zinc finger protein, zic, is involved in neurogenesis, especially in the cell lineage of cerebellar granule cells. J Neurochem. 1994; 63:1880–90. [PubMed: 7931345]
8. Zhu J, Nakamura E, Nguyen MT, Bao X, Akiyama H, Mackem S. Uncoupling sonic hedgehog control of pattern and expansion of the developing limb bud. Dev Cell. 2008; 14:624–32. [PubMed: 18410737]
9. Quinn ME, Haaning A, Ware SM. Preaxial polydactyly caused by Gli3 haploinsufficiency is rescued by Zic3 loss of function in mice. Hum Mol Genet. 2012; 21:1888–96. [PubMed: 22234993]
10. Kitaguchi T, Nagai T, Nakata K, Aruga J, Mikoshiba K. Zic3 is involved in the left-right specification of the Xenopus embryo. Development. 2000; 127:4787–95. [PubMed: 11044394]
11. Purandare SM, Ware SM, Kwan KM, et al. A complex syndrome of left-right axis, central nervous system and axial skeleton defects in Zic3 mutant mice. Development. 2002; 129:2293–302. [PubMed: 11959836]

12. Ware SM, Harutyunyan KG, Belmont JW. Heart defects in X-linked heterotaxy: evidence for a genetic interaction of Zic3 with the nodal signaling pathway. Dev Dyn. 2006; 235:1631–7. [PubMed: 16496285]
13. Carrel T, Purandare SM, Harrison W, et al. The X-linked mouse mutation Bent tail is associated with a deletion of the *Zic3* locus. Hum Mol Genet. 2000; 9:1937–42. [PubMed: 10942421]
14. Czosek RJ, Haaning A, Ware SM. A mouse model of conduction system patterning abnormalities in heterotaxy syndrome. Ped Res. 2010; 68:275–80.
15. Cast AE, Gao C, Amack JD, Ware SM. An essential and highly conserved role for Zic3 in left-right patterning, gastrulation and convergent extension morphogenesis. Dev Biol. 2012; 364:22–31. [PubMed: 22285814]
16. Chhin B, Hatayama M, Bozon D, et al. Elucidation of penetrance variability of a ZIC3 mutation in a family with complex heart defects and functional analysis of ZIC3 mutations in the first zinc finger domain. Hum Mutat. 2007; 28:563–70. [PubMed: 17295247]
17. Chung B, Shaffer LG, Keating S, Johnson J, Casey B, Chitayat D. From VACTERL-H to heterotaxy: variable expressivity of ZIC3-related disorders. Am J Med Genet A. 2011; 155A: 1123–8. [PubMed: 21465648]
18. De Luca A, Sarkozy A, Consoli F, et al. Familial transposition of the great arteries caused by multiple mutations in laterality genes. Heart. 2010; 96:673–7. [PubMed: 19933292]
19. Megarbane A, Salem N, Stephan E, et al. X-linked transposition of the great arteries and incomplete penetrance among males with a nonsense mutation in ZIC3. Eur J Hum Genet. 2000; 8:704–8. [PubMed: 10980576]
20. Zhu L, Harutyunyan KG, Peng JL, Wang J, Schwartz RJ, Belmont JW. Identification of a novel role of ZIC3 in regulating cardiac development. Hum Mol Genet. 2007; 16:1649–60. [PubMed: 17468179]
21. Ware SM, Harutyunyan KG, Belmont JW. Zic3 is critical for early embryonic patterning during gastrulation. Dev Dyn. 2006; 235:776–85. [PubMed: 16397896]
22. Hashimoto K, Nakatsuji N. Formation of the primitive streak and mesoderm cells in mouse embryos - detailed scanning electron microscopical study. Dev Growth Differ. 1989; 31:209–18.
23. Tam PPL, Behringer RR. Mouse gastrulation: the formation of a mammalian body plan. Mech Dev. 1997; 68:3–25. [PubMed: 9431800]
24. Takeuchi JK, Ohgi M, Koshiba-Takeuchi K, et al. Tbx5 specifies the left/right ventricles and ventricular septum position during cardiogenesis. Development. 2003; 130:5953–64. [PubMed: 14573514]
25. Koshiba-Takeuchi K, Mori AD, Kaynak BL, et al. Reptilian heart development and the molecular basis of cardiac chamber evolution. Nature. 2009; 461:95–8. [PubMed: 19727199]
26. Oyen N, Poulsen G, Boyd HA, Wohlfahrt J, Jensen PK, Melbye M. Recurrence of congenital heart defects in families. Circulation. 2009; 120:295–301. [PubMed: 19597048]
27. Meyers EN, Lewandoski M, Martin GR. An Fgf8 mutant allelic series generated by Cre- and Flp-mediated recombination. Nat Genet. 1998; 18:136–41. [PubMed: 9462741]
28. Lowe LA, Yamada S, Kuehn MR. Genetic dissection of nodal function in patterning the mouse embryo. Development. 2001; 128:1831–43. [PubMed: 11311163]
29. Saijoh Y, Oki S, Ohishi S, Hamada H. Left-right patterning of the mouse lateral plate requires nodal produced in the node. Dev Biol. 2003; 256:160–72. [PubMed: 12654299]
30. Warburton D, El-Hashash A, Carraro G, et al. Lung organogenesis. Curr Top Dev Biol. 2010; 90:73–158. [PubMed: 20691848]
31. Constam DB, Robertson EJ. SPC4/PACE4 regulates a TGFbeta signaling network during axis formation. Genes Dev. 2000; 14:1146–55. [PubMed: 10809672]
32. Meno C, Shimono A, Saijoh Y, et al. lefty-1 Is Required for Left-Right Determination as a Regulator of lefty-2 and nodal. Cell. 1998; 94:287–97. [PubMed: 9708731]
33. Tsukui T, Capdevila J, Tamura K, et al. Multiple left-right asymmetry defects in Shh(−/−) mutant mice unveil a convergence of the shh and retinoic acid pathways in the control of Lefty-1. Proc Natl Acad Sci U S A. 1999; 96:11376–81. [PubMed: 10500184]

34. Jiang Z, Zhu L, Hu L, et al. Zic3 is required in the extra-cardiac perinodal region of the lateral plate mesoderm for left-right patterning and heart development. Hum Mol Genet. 2013; 22:879–89. [PubMed: 23184148]

35. Sutherland MJ, Wang S, Quinn ME, Haaning A, Ware SM. Zic3 is required in the migrating primitive streak for node morphogenesis and left-right patterning. Hum Mol Genet. 2013

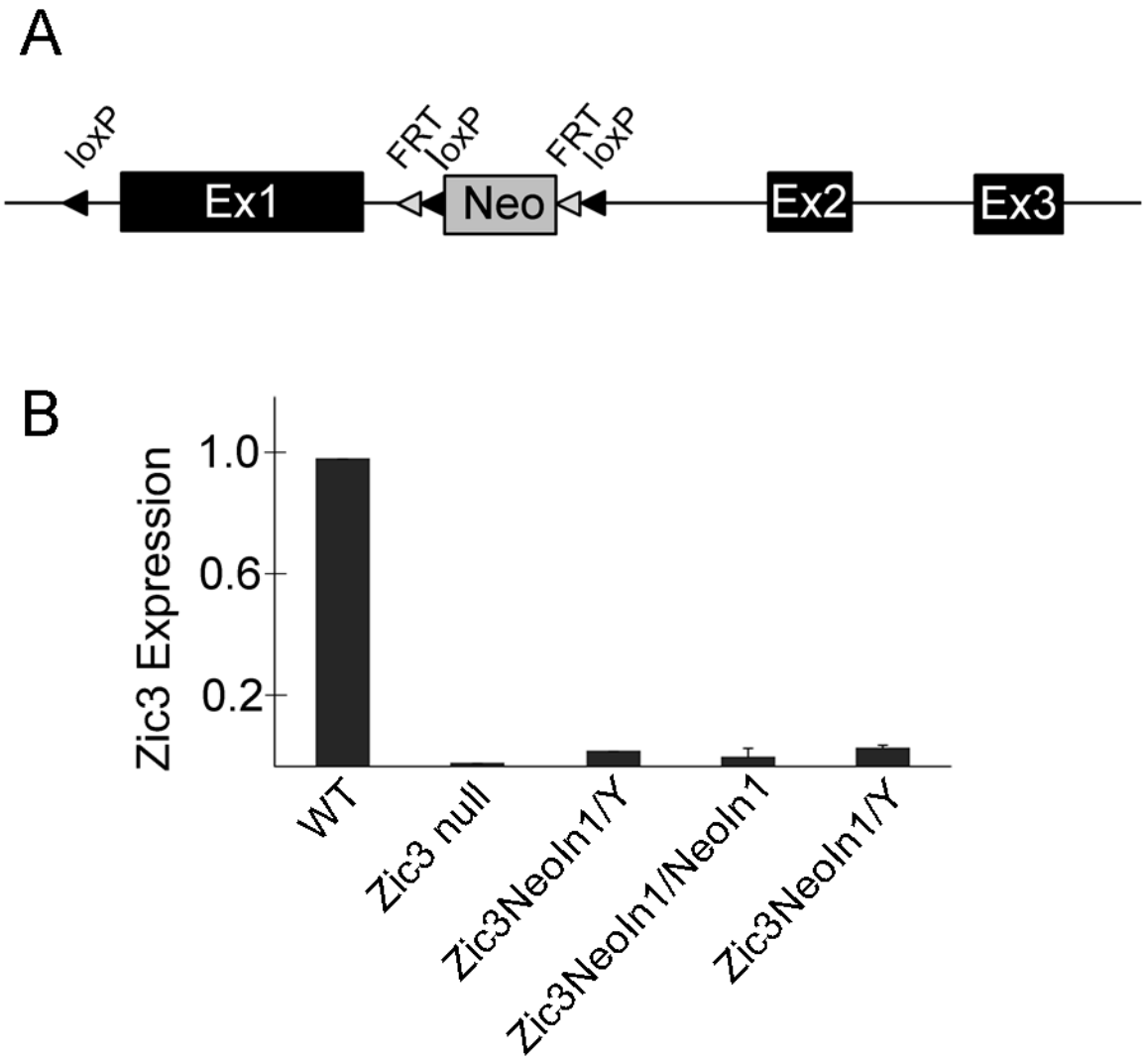

Figure 1.

Disruption of intron 1 of *Zic3* results in a hypomorphic $Zic3^{NeoI1}$ allele. A neomycin cassette was incorporated into intron 1 of mouse Zic3 by targeted insertion (A). The resulting $Zic3^{NeoIn1}$ allele exhibited reduced *Zic3* expression by qPCR (B). Each bar in the qPCR graph (B) represents *Zic3* expression level in one embryo of the indicated genotype. Null embryos are hemizygous if male ($Zic3^{NeoIn1/Y}$) and homozygous if female ($Zic3^{NeoIn1/NeoIn1}$).

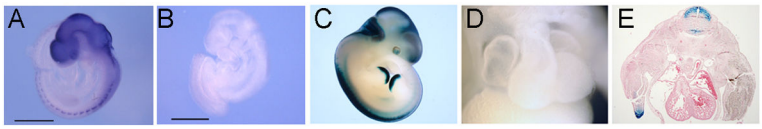

Figure 2.

Analysis of *Zic3* expression in the mouse embryo. *Zic3* expression is visualized in the WT embryo by whole mount in situ hybridization (A) and is not detectable by WISH in Neo embryos (B). Analysis of *Zic3* expression using *Zic3*-LacZ-BAC transgenic mice (C) revealed no expression in the heart grossly (D) or histologically (E). Neo: $Zic3^{NeoIn1/NeoIn1}$ or $Zic3^{NeoIn1/y}$. Scale bars in A and B: 0.5 mm.

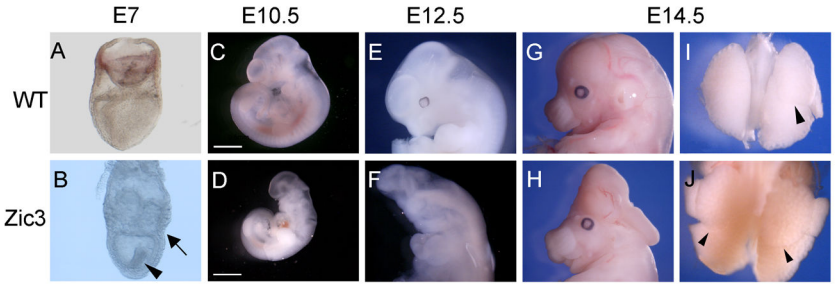

Figure 3.

Representative phenotypes of *Zic3* hypomorphs at different stages. Gastrulation abnormalities were observed in some hypomorphic embryos (B, arrow, arrowhead; compare to wild type embryo in A). Growth retardation was common in hypomorphs, compared to wild-type siblings (C, wild type; D, hypomorph). Neural tube defects were observed in many hypomorphs (F, H; compare to wild type in E, G). Laterality defects such as right isomerism occurred frequently, indicated here by bilateral, multilobed lungs (J, arrowheads; compare to wild type in I). Scale bars, 0.5 mm.

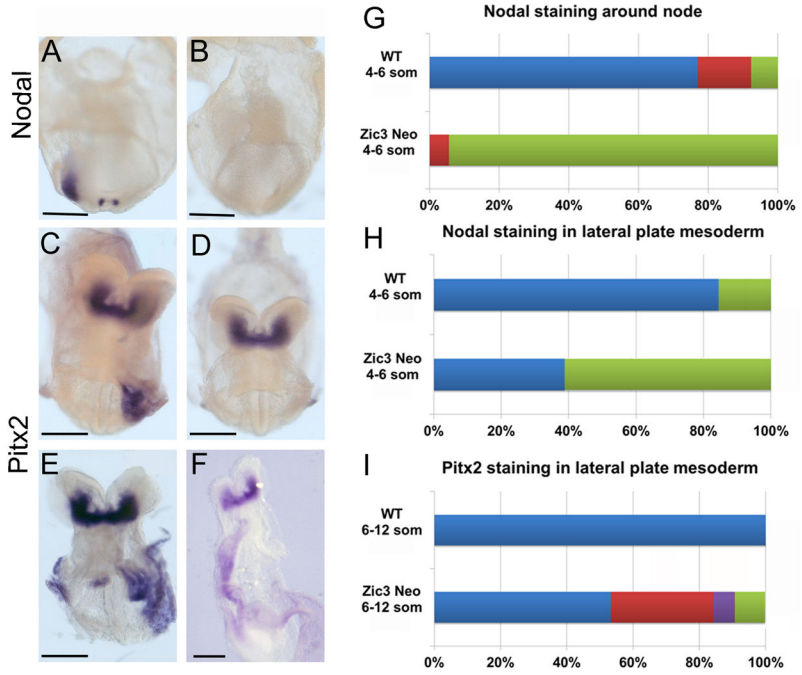

Figure 4.

Abnormal left-right marker expression in *Zic3* hypomorphs. WISH using a nodal riboprobe demonstrates bilateral, perinodal and left lateral plate mesoderm (LPM) staining in four-somite stage wild-type (WT) embryo (A) compared to four-somite stage *Zic3* hypomorphic embryo with absent staining (B). Left LPM *Pitx2* expression in WT ten-somite stage embryo (C). Variable *Pitx2* staining patterns in eight- to ten-somite *Zic3* hypomorphs: absent (D), bilateral (E), and right LPM (F). *Nodal* staining patterns observed around the node in WTs and *Zic3* hypomorphs (G; WT n=13, hypomorph n=18). Blue color represents left>right staining of node; Red color represents bilaterally equal expression at the node; green represents absent staining at the node. *Nodal* staining patterns observed in LPM of WTs and *Zic3* hypomorphs (H; WT n=13, hypomorph n=18). Blue color represents left LPM staining; green represents absent LPM staining. *Pitx2* staining patterns observed in LPM of WTs and *Zic3* hypomorphs (I; WT n=29; hypomorph n=45). Blue color represents left LPM staining; green represents absent LPM staining; red represents bilateral LPM staining; purple represents right LPM staining. Scale bars, 100 μm.

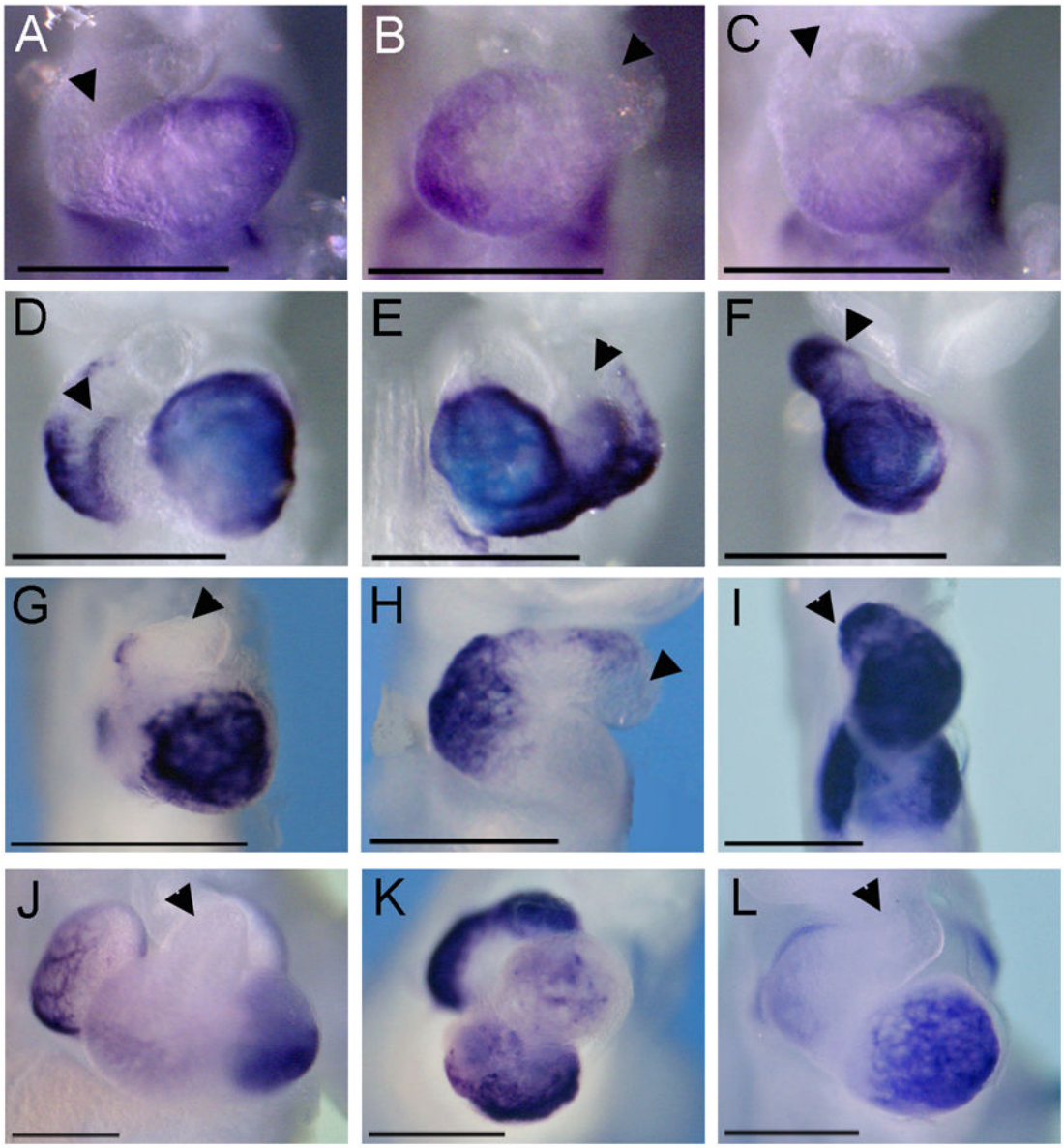

Figure 5.

Markers of cardiac differentiation are expressed normally, despite complex looping defects. E9.5 embryos (A–I) and E11.5 embryos (J–L) were analyzed for markers of cardiac differentiation, *Tbx5* and *Nppa*. Tbx5 (A–C) was expressed in all *Zic3* null and hypomorphic embryos analyzed, and the level of expression was comparable to wild-type expression levels (A, D, J). *Tbx5* was normally localized to the proper morphological location in *Zic3* null embryos (B, C), despite looping abnormalities. *Nppa* (D–L) was normally localized to the proper morphological location in *Zic3* null (E, F) and hypomorphic embryos (H, I, K, L), despite looping abnormalities. For comparison, see Nppa in wild-type embryos at E9.5 (D) and E11.5 (J). Arrowheads, outflow tract. Scale bars, 6× magnification.

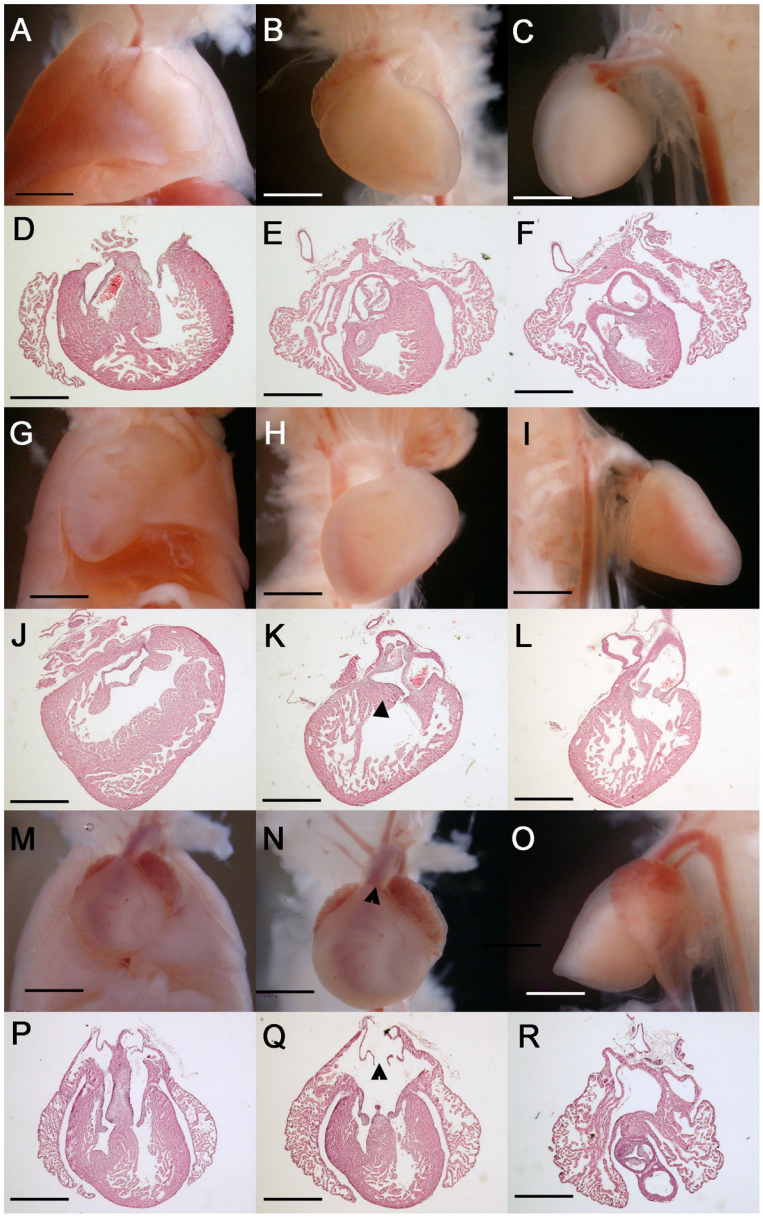

Figure 6.

Complex cardiovascular malformations in E17.5 *Zic3* hypomorphs. Gross and histologic transverse sections from wild-type E17.5 embryos (A–F) and *Zic3* hypomorphs (G–R). Wild type embryos have levocardial positioning in chest (frontal view, A) and proper orientation of chambers and great arteries (B, C frontal and lateral views, D–F transverse sections). A representative *Zic3* hypomorphic embryo (G–L) demonsrates dextrocardial positioning in the chest (G) with right aortic arch (H, I frontal and lateral views) and DORV (J–L) with subaortic VSD (K, triangle). Another *Zic3* hypomorphic embryo had mesocardial positioning in the chest (M), atrial isomerism, TGA, and an anteriorly-positioned aorta (N, triangle; O). Transverse sections demonstrate these defects as well as AVSD (P–R) and symmetrical venous valves (Q, triangle). All sections are in transverse plane, shown

posterior to anterior. DORV, double-outlet right ventricle. VSD, ventricular septal defect. AVSD, atrioventricular septal defect. TGA, transposition of the great arteries. Scale bars, 2× magnification.

Table 1

Analysis of genotype and phenotype at different developmental stages

Genotype	Phenotype	E8.5–9.5	Percent of total offspring[a]	E10.5–11.5	Percent of total offspring[a]	E12.5–14.5	Percent of total offspring[a]	E17.5	Percent of total offspring[a]
$Zic3^{WT/y}$	Normal	30	23	23	23	20	26	12	26
	Abnormal	-		-		1		-	
$Zic3^{NeoIn1/WT}$	Normal	36	27	25	26	23	28	15	3
	Abnormal	-		-		-		1	
$Zic3^{NeoIn1/NeoIn1}$	Normal	16	25	10	28	12	26	2	17
	Abnormal	17		17		9		6	
$Zic3^{NeoIn1/y}$	Normal	20	26	15	23	8	21	5	22
	Abnormal	14		8		9		5	
Totals		133		98		82		46	
# Litters		13		11		11		6	

[a]Theoretical frequencies are 25% for each genotype at all stages

Table 2

Reduction in Zic3 expression results in an array of heart defects

E9-9.5 Number of embryos (n)	**13**	**4**	**2**	**1**	**1**	**% of Total n=21**
Normal	+					62%
Simple tube		+			+	24%
L-looped			+			10%
Partially looped				+		5%
Situs abnormality					+	5%

E10.5–11.5 Number of embryos (n)	**28**	**5**	**3**	**3**	**2**	**2**	**2**	**1**	**1**	**1**	**1**	**% of Total n=49**
Normal	+											57%
Inferior/superior ventricles		+				+				+		16%
Single ventricle			+	+			+		+			18%
Simple tube				+	+							10%
L-looped						+	+	+	+	+		14%
Situs abnormality								+	+	+	+	8%
Pericardial edema				+	+							10%

E12.5–14.5 Number of embryos (n)	**15**	**1**	**1**	**1**	**1**	**1**	**1**	**% of Total n=49**
Normal	+							71%
Interior/superior ventricles		+				+		10%
Single ventricle				+				5%
Single atrium			+	+				10%
L-looped					+	+		10%
Pericardial edema						+	+	10%

Pediatr Res. Author manuscript; available in PMC 2014 September 27.

Table 3

Phenotypes of E17.5 Zic3 hypomorphs from six litters

Number of embryos	Overall Phenotype	Cardiac Phenotype
7	Normal (situs solitus)	Normal (levocardia)
1	Exencephaly. Normal otherwise.	Normal (levocardia)
1	Right pulmonary isomerism; asplenia, stomach on left	Mesocardia, TGA, right atrial isomerism, AVSD and symmetrical venous valves
1	Right pulmonary isomerism; asplenia. Stomach on right. Intestines malpositioned outside of liver. Anal atresia	Mesocardia, TGA, right atrial isomerism, AVSD and symmetrical venous valves
1	Right pulmonary isomerism; asplenia. Stomach large and centrally-located.	Mesocardia, TGA, right atrial isomerism, AVSD and symmetrical venous valves
1	Situs ambiguus. Lungs abnormally multi-lobed but not symmetrical.	DORV with VSD. Normal otherwise (levocardia)
1	Situs ambiguus. Lungs abnormally multi-lobed but not symmetrical. Intestinal atresia.	Bottom of heart flat. Single ventricle. Single atrium (right). Only one set of A/V valves. Right descending aorta. Anteriorly-positioned aorta.
1	Situs ambiguus. Lungs abnormally multi-lobed but not symmetrical. Severe exencephaly & anterior neural tube closure defect. Microcephaly and facial malformations (low ears, no eyes).	Mesocardia, large RA, small LA. AVSD. Right descending aorta.
1	Situs ambiguus. Lungs abnormally multi-lobed but not symmetrical. Severe exencephaly & anterior neural tube closure defect. Microcephaly and facial malformations (low-set ears, no eyes). Rib dysplasia.	Large RA, small LA. AVSD. Right descending aorta. TGA.
1	Situs ambiguus. Lungs abnormally multi-lobed but not symmetrical. Severe exencephaly & anterior neural tube closure defect. Microcephaly and facial malformations (low-set ears, no eyes). Rib dysplasia.	AVSD. Right descending aorta. TGA.
1	Pulmonary and abdominal situs inversus.	Dextrocardia. Anteriorly-positioned aorta. DORV with subaortic VSD.
1	Pulmonar and abdominal situs inversus; Microphthalmia.	Dextrocardia. Anteriorly-positioned aorta. DORV with subaortic VSD.